Cite this chapter as:
Brainerd, E.L. and M.E. Hale. 2006. In vivo and functional imaging in developmental physiology.
In Comparative Developmental Physiology, S. Warburton and W. Burggren, eds.
Oxford University Press, pages 21-40.

2

In Vivo and Functional Imaging in Developmental Physiology

ELIZABETH L. BRAINERD
MELINA E. HALE

Recent advances in functional and in vivo imaging provide powerful tools for the study of developmental physiology. Techniques such as confocal microscopy, magnetic resonance microscopy (MRM), microtomography (microCT), and ultrasound microscopy allow developmental physiologists to collect high-resolution images of living embryos and larvae. In vivo imaging techniques can be applied repeatedly over time, allowing longitudinal studies of development in the same individual (Fenster 2002).

Imaging techniques are ideal for visualizing anatomical structures, from which aspects of function can be inferred, and these techniques have also been adapted to measure physiological performance directly. For example, changes in regional blood flow (Schwerte et al. 2003), cardiac output (Hove et al. 2003), and activity of specific neurons (Ritter et al. 2001) can be monitored in vivo. Imaging techniques that allow simultaneous measurement of structure and function facilitate the integration of morphological and physiological perspectives on development.

In vivo imaging techniques make it possible to do perturbation experiments on embryos. With repeated imaging of the same individual, it is possible to measure some aspect of physiological performance, disrupt the system, for example with microinjection of drugs or laser ablation of specific cells, and then measure performance again. Comparative physiologists have a great deal of expertise designing and performing perturbation experiments, and this expertise can now be brought to bear on the physiology of developing organisms.

The integration of developmental physiology with studies of gene expression and function is also facilitated by new imaging techniques. Imaging gene expression in vivo is increasingly possible with transgenic coexpression of fluorescent proteins along with genes of interest (e.g., Stuart et al. 1988; Higashijima et al. 1997, 2000). Fluorescent

transgenic lines provide powerful tools that can be used to image morphology in mutants and when gene products are experimentally manipulated. In addition, fluorescent proteins make it possible to target particular cell types for physiology or lesioning experiments.

Functional, in vivo imaging places enormous demands on imaging technologies. Ideally we should like to have what some have called 5D imaging: 3D images collected over time with spectral (color) information indicating specific structures, functions, or gene expression patterns (Swedlow et al. 2003). High spatial resolution, generally 10 μm or better, is required for imaging small life stages. Some applications require very high temporal resolution, 1 ms (1000 images per second) or higher, but many studies in developmental physiology would be well served by "real-time" imaging at 20–30 frames per second.

All of the imaging techniques available today are limited in their ability to collect 5D information. High-resolution 3D images can be collected, but a complete 3D scan of a specimen takes a relatively long time, limiting 3D imaging to time-lapse recording of slow-changing phenomena. In both 2D and 3D imaging, images with higher spatial resolution take longer to collect, thereby creating a tradeoff between spatial and temporal resolution. Other limitations of imaging techniques for developmental physiology are that specimens generally need to be immobilized, specimens must be transparent for the optical methods, and some techniques are limited in how deeply they can penetrate into a specimen.

Image Informatics

The use of multidimensional images as a primary data source creates problems as well as opportunities in the analysis, storage, and sharing of large image datasets (Shotton 2000; Marx 2002; Barinaga 2003; Swedlow et al. 2003). Powerful image analysis programs allow quantitative data to be extracted from images, but researchers must agree on sets of standards for image processing, analysis, and the reporting of image manipulation. High-capacity data storage devices make it possible to store and archive large numbers of images, and many images are often collected and stored for every image that appears in journal articles. However, the detailed information needed for the subsequent analysis of these images, such as magnification, frame rate, optical slice thickness, image processing, and experimental details, is often lost.

Several groups of biologists and computer scientists are working on image database projects (Shotton 2000; Marx 2002; Barinaga 2003; Swedlow et al. 2003). These projects emphasize that standards for recording metadata about images, such as details about the specimen and how the image was captured and processed, are central to this effort. These standards may be analogous to the Minimum Information About a Microarray Experiment (MIAME) standards in that they should provide enough information for a researcher to evaluate the quality of the data and to reanalyze them. The development of image database standards will also benefit individual researchers, as these databases could be used to manage images within a research group and reduce unnecessary duplication of effort.

A few journals are beginning to require that images be deposited in public databases, just as most journals require that gene sequences be deposited. An early adopter of

this requirement was the *Journal of Cognitive Neuroscience*, which requires that all brain images captured by functional MRI (fMRI) be deposited in a public database at Dartmouth College (www.fmridc.org; Barinaga 2003). Other major image informatics projects include the Open Microscopy Environment (http://www.openmicroscopy.org; Swedlow et al. 2003) and the BioImage Database project (www.bioimage.org; Shotton 2000). Physiology journals that currently publish image-intensive papers should consider the requirement that images be deposited in a database, and if a developmental physiology journal is started, the editors should require image deposition.

Labeling Techniques

When we think about technical developments in imaging, we tend to think about new image acquisition hardware and perhaps sophisticated image processing and quantitative analysis software. However, the development of new and clever ways to label biological structures and functions has proven to be just as important in the development of in vivo imaging. Labeling techniques increase the ability to distinguish between structures and sometimes provide functional information about gene expression or the physiological state of the tissues under study (such as calcium-sensitive dyes that fluoresce when neurons are active). The general term used to refer to labeling materials—contrast agents, labels, probes, markers, indicators, stains, and dyes—varies depending on whether their developers come from radiology, molecular biology, or microscopy backgrounds.

Some of the simplest and most generally applicable labeling methods are microinjection, histochemistry, and immunohistochemistry. The microinjection of fluorescent labels directly into regions of interest has been particularly successful for in vivo confocal imaging of neuron structure and function in zebrafish (e.g., Hale et al. 2001; Ritter et al. 2001). Microinjection can be combined with photoactivated fluorescent proteins for even more spatially specific labeling (Chudakov et al. 2003). A light-sensitive chromoprotein is injected into the general area of interest and then a laser is used to kindle (activate) the chromoprotein in a very specific area. Different wavelengths of laser light can cause reversible kindling, quenching of reversible kindling, and irreversible kindling (Chudakov et al. 2003).

Histochemistry and immunohistochemistry can be used to identify specific tissues or cells based on their chemical and immunological reactivity. Immunostaining can be quite specific, for example, distinguishing between slow and fast myosins (e.g., Barresi et al. 2001; Hernandez et al. 2002). Secondary labels for fluorescence or transmitted light microscopy can be used, and the development of fluorescent quantum dots (semiconductor nanocrystals) shows great promise (Seydel 2003). Fluorescent dye labels fade relatively quickly and are subject to photobleaching from laser excitation, and multilabel preparations must be excited at multiple wavelengths to produce multicolored emission spectra. Quantum dots, on the other hand, can persist for weeks without harming living tissue, are resistant to photobleaching, and different-sized crystals (1–10 nm) produce a range of colors with excitation at just one wavelength (Dubertret et al. 2002). Quantum dots have been used successfully to track cell fate in developing frog embryos (Dubertret et al. 2002), antibodies can be conjugated to quantum dots for immunostaining (Goldman et al. 2002), and DNA can be conjugated to quantum dots to hybridize with specific sequences in vivo (Dubertret et al. 2002).

Other methods can be used to label gene expression. In situ hybridization, which targets the mRNA of specific genes, is only applicable to fixed tissues. However, transgenic techniques make it possible to coexpress a label (reporter) gene along with the gene of interest. The most commonly used protein for in vivo imaging of gene expression is green fluorescent protein (GPF) from a jellyfish, and bioluminescent luciferase labels from fireflies and other animals have also been developed recently (O'Connell-Rodwell et al. 2002). Progress has also been made in developing radionuclide and magnetic-based reporter systems for PET and MRI imaging of gene expression (MacLaren et al. 2000).

For comparative work on nonmodel species, microinjection and histochemistry are the most broadly applicable techniques. Antibodies for immunostaining are highly cross-reactive, with mammalian antibodies sometimes working well in fishes and amphibians (Hanken et al. 1992; Hernández et al. 2002). However, it is generally the case that cross-reactivity is most reliable in closely related species. Transgenic techniques for in vivo labeling of gene expression are currently more suited to studies of model organisms than to broadly comparative studies.

Overview of In Vivo Imaging Methods

Below we provide a brief overview of imaging methods appropriate for embryos, larvae, and fetuses in vivo. Many of these are also appropriate for living cells in tissue culture and living slice preparations of brains, but we do not specifically address issues related to these in vitro preparations. Some key features of different imaging techniques are summarized in table 2.1.

Digital Photomicroscopy

Standard digital photomicroscopy is sometimes called widefield optical photomicroscopy to distinguish it from other optical methods (such as confocal). A wide field of view is imaged all at once, generally with a high-resolution, cooled CCD camera. Cooling the CCD with liquid nitrogen reduces noise, and allows longer exposures for low light applications (especially fluorescence). This technique is most commonly used to collect 2D images, but can be combined with optical sectioning and deconvolution to produce 3D digital reconstructions. For in vivo 3D imaging, the subject must be optically clear and immobilized. This is probably most practical for small, transparent invertebrates and vertebrates such as zebrafish embryos and larvae. The structures of interest must be labeled or otherwise distinguishable from surrounding tissues (fluorescent labels work well). Then the focal plane, often controlled by a motorized stage, is moved in known increments and an image is taken at each depth (optical sectioning). Deconvolution is then used to remove the out-of-focus information from each section, and the sections are combined into one set of aligned (registered) images, called a z-stack or z-series.

A 3D reconstruction program can then be used to reconstruct voxels (3D pixels) from the 2D section pixel information and optical section thickness (from the movements of the motorized stage). A true, 3D digital reconstruction can be visualized as a volumetric rendering, can be rotated in 360° around all axes, and can be resectioned in

Table 2.1 Summary of in vivo imaging methods

Imaging method	Spatial resolution	Transparent specimen required?	Special labeling or contrast agents	Generally used for 3D[a]	Time resolution[b]
Digital photomicroscopy	0.3 μm	Yes	Optional	No	Poor
Videomicroscopy	Good[c]	Yes	Optional	No	33–40 ms[d] 1 ms[e]
Laser scanning confocal	0.3 μm	Yes	Required (fluorescent)	Yes	2 ms per line scan 300 ms per section[f]
Optical projection tomography (OPT)	0.3 μm	Yes	Optional	Yes	Currently poor
MR microscopy	10 μm	No	Optional	Yes	80 ms per section
MicroCT	10 μm	No	Optional	Yes	100 ms per section
Synchrotron beam microscopy	1 μm	No	Optional	No	10 ms per section
Ultrasound microscopy	50 μm	No	Optional	No	100 ms per section
Optical coherence tomography (OCT)	5 μm	Preferred	Optional	Yes	100 ms per section
Positron emission tomography (PET)	1 mm	No	Required (positron emitting)	Yes	Poor

[a]Multiple image sections from most of these methods can be used for 3D reconstruction; we note whether the technique is usually used this way or not.

[b]Time resolution depends on spatial resolution; values presented are for resolutions lower than the maximum possible for a given method.

[c]Resolution depends on the resolution of the video camera: cooled CCD cameras provide the best resolution, high-speed video cameras generally have lower resolution.

[d]The NTSC video standard is 30 frames per second (fps) and PAL video is 25 fps. Time lapse allows collection of images over longer periods of time at lower frame rates.

[e]Many high-speed video systems have a maximum frame rate of 1000 fps. Systems are available with higher frame rates, but 1000 fps is often the practical limit because of the increasing amount of light required with increasing frame rate.

[f]Better time resolution can be achieved with spinning disk (Nipkow disk) confocal systems.

any plane. The resolution of the resectioned slices depends on the resolution of the 2D slices and the thickness of the slices. A mismatch between the pixel resolution of the 2D image and the section thickness produces rectangular voxels. Slice thickness is generally greater than 2D slice resolution, so it often makes sense to downsample the 2D slices for consistent resectioning results.

Videomicroscopy

Videomicroscopy allows higher temporal resolution, generally by sacrificing spatial resolution. The exception is time-lapse video of relatively slow movements, which can allow high-resolution images to be collected. Videomicroscopy is particularly suited to measuring rapidly changing physiological parameters in vivo, such as blood flow and cardiac and muscle function. An in vivo and completely noninvasive technique for imaging the circulatory system in larval zebrafish was recently developed, along with methods for measuring blood cell concentration and blood distribution from videomicroscopy (Schwerte et al. 2003). In another recent paper (Hove et al. 2003), intracardiac fluid forces in the developing heart of zebrafish were estimated from digital particle

image velocimetry (DPIV) of blood cells moving in 440–1000 frames per second high-speed videos.

Laser Scanning Confocal Microscopy

Laser scanning confocal microscopy is an extremely effective method for 3D imaging of fluorescent labels in small, transparent embryos in vivo. A laser is focused to excite fluorescence in a small voxel of the tissue, and a pinhole aperture on the microscope limits the recorded light to an even more specific region. The laser and pinhole move along a line to create a line scan, and then line scans are built up into sections, and the sections into 3D reconstructions.

Standard confocal microscopy can only image labeled structures to a depth of about 1 mm; below this depth, too much of the laser light is absorbed by the intervening tissue (Stephens and Allan 2003). Greater depths can be imaged with two-photon and multiphoton confocal microscopy. In two- and multiphoton confocal imaging, longer wavelength pulses of infrared laser light are used for excitation. Infrared photons have less energy than visible light photons, so two or more photons must be absorbed within a femtosecond for the label to fluoresce. The longer wavelength lasers penetrate deeper into the tissue, up to 5 mm, because they are scattered and absorbed less than visible light lasers. They also have lower energy, so they cause less photobleaching of the label and less photodamage to the organism (Stephens and Allan 2003). Skin pigment interferes with all forms of confocal imaging. Early embryos generally image well owing to the absence of pigment, and albino strains can be useful for imaging later stages.

The time resolution of confocal imaging depends on the speed at which the laser scans through the tissue and the amount of information required for a particular application. For example, a line scan through the cell body of a neuron labeled with a calcium-sensitive dye is sufficient to determine the activity level of the neuron (Ritter et al. 2001). Line scans can be collected at a rate of 500 s^{-1}, or 2 ms time resolution. A typical 2D laser scanning confocal section can be collected in about 300 ms, and the time required for a full z-stack for 3D reconstruction is the time per section times the number of sections (100 sections would require 30 seconds). Time-lapse 3D imaging is possible, but real-time (at least 20 frames per second) 4D imaging is not yet possible with laser scanning confocal.

Spinning disk (also called Nipkow disk) confocal is a method designed to increase the scanning rate. The excitation laser is broken into multiple foci by microlenses on a spinning disk. Confocality is achieved with a second spinning disk containing a series of pinholes. In this way, multiple voxels can be sampled at once. Spinning disk systems can achieve standard video speeds of up to 30 frames per second, and can be modified for higher speed capture.

Some clever methods have been developed to use photobleaching and other effects of laser light on the fluorescent labels to image function in live cells and tissues. These techniques are named with an alphabet soup of acronyms, biased strongly in favor of F-words—FRAP, FLIP, FLIM, and FRET (Stephens and Allan 2003). The mobility of fluorochrome-tagged proteins can be measured with fluorescence recovery after photobleaching (FRAP) and fluorescence loss in photobleaching (FLIP). Both involve deliberately photobleaching an area, and then measuring how long it takes for fluorescence to be recovered in the bleached area (FRAP), or repeatedly bleaching an area and

measuring how long it takes for adjacent areas to become bleached (FLIP). Fluorescence lifetime imaging (FLIM) provides a way to distinguish between fluorochromes with similar emission spectra but different fluorescence lifetimes. Fluorescence resonance energy transfer (FRET) has been useful for measuring calcium flux in vivo. In calcium imaging using FRET biosensor labels, energy is transferred from one fluorochrome to a spectrally overlapping but distinct fluorochrome in the presence of calcium. A change in the emission spectrum signals the presence of calcium. To increase the sensitivity of FRET, FLIM can be used to help distinguish between fluorochromes with similar emission spectra (Stephens and Allan 2003).

Optical Projection Tomography

Optical projection tomography (OPT) was developed as an alternative to confocal microscopy for 3D imaging of larger specimens (particularly mouse embryos; Sharpe et al. 2002). The specimen is embedded in an agar cylinder, and rotated slowly through 360° while projected light through the specimen is collected in multiple views and at multiple section levels. Tomography (the calculation of 3D information from 2D information) is then used to reconstruct sections and 3D volumes. Unlike confocal, specimens up to 1 cm thick can be imaged and the technique works with nonfluorescent as well as fluorescent labels. The drawback is that the specimen must be optically clear and completely immobilized for a long period of time. In vivo imaging of small, transparent embryos may be possible, but larger embryos must be killed and cleared with chemical clearing agents.

MR Microscopy

Magnetic resonance imaging (MRI) has become an important tool for imaging soft tissues in the human body, and in recent years, MR scanners have been developed with sufficient resolution to image small animals and embryos (Bulte et al. 2002). The maximum resolution of MR microscopy (MRM) is 10 μm, with 20 μm being more typical. Scanners designed for human diagnostics generally use relatively low magnetic fields of 1–3 Tesla (T), whereas the higher resolution scanners for MRM operate at 5–7 T. Confocal and widefield microscopy yield higher resolution images and therefore are better than MRM for imaging small, clear, easily accessible embryos, but MRM is particularly suitable for large, inaccessible embryos such as those of mammals and birds.

In magnetic resonance imaging, intrinsic contrast between tissues comes primarily from differences in proton density due to differences in water concentration. Fatty tissues, which have low water contents, are most clearly distinguishable from other soft tissues. Intrinsic contrast can also arise from differences in magnetic relaxation times, which depend on the chemical composition of bound or free water protons in the tissues. Scans can be weighted to emphasize different components of magnetic relaxation, T_1 (longitudinal relaxation), T_2 (transverse relaxation), or T_2^* (transverse relaxation without compensation for dephasing spins) (Bulte et al. 2002). Diffusion tensor imaging, based on directional water diffusion, can sometimes be used to detect the presence and orientation of fibers within a tissue, such as axon bundles, connective tissues, and muscle fibers (Bulte et al. 2002). Functional MRI (fMRI) has been used extensively to

image brain activity in humans and small animals, based on changes in blood flow and the blood oxygen level dependent (BOLD) fMRI technique (Logothetis et al. 2001).

When intrinsic tissue MR contrast is not sufficient, extrinsic contrast agents may be administered. Most of these agents have been developed for use in medical MRI, so they have low toxicity and are compatible with long-term in vivo studies. Paramagnetic contrast agents, usually gadolinium, create hyperintense (bright) contrast on T_1-weighted images and superparamagnetic iron oxide (SPIO) nanoparticles generate hypointense (dark) contrast on T_2^*-weighted images (Bulte et al. 2002). Contrast agents have been used to track cell movements and cell fate in developing frog embryos (Jacobs and Fraser 1994), and extensive work is currently under way to develop MR contrast agents for gene expression (e.g., Louie et al. 2000). Hyperpolarized ^{3}He gas is an effective MRM contrast agent for studies of fine-scale airway structures in lungs (Chen et al. 1998).

Specimens must be immobilized, usually by anesthesia, for MRM because a complete 3D scan can take many minutes to collect. Temporal gating is used to filter out respiratory and sometimes cardiac movements. In temporal gating, sections are collected in the same phase of the cardiac or respiratory cycle over several cycles, and then reconstructed into a single 3D image. By collecting a series of images gated across all phases of the respiratory or cardiac cycle, a time series of 3D images can be reconstructed, creating 3D movies of cyclical events (Chen et al. 1998; Alley et al. 1999). This gated, cineMRI technique approaches the goal of 4D imaging, but the movies are composites of many heartbeats or breaths, rather than true 3D images collected in real time. Therefore, 3D cineMRI is suitable for the study of highly repeatable, cyclical movements, but not suitable for variable cyclic or phasic movements.

Microtomography

The resolution of clinical x-ray CT scans, about 1 mm, is not high enough for most applications in developmental physiology. High resolution x-ray CT imaging (microtomography or microCT) has been developed for scanning nonliving materials in industry, with resolution down to 1 μm. MicroCT has been adapted for use in living animals, but the need to keep x-ray doses low for repeated imaging of living animals over time limits the resolution of in vivo microCT to about 10 μm (Holdsworth et al. 2002; DeClerck et al. 2003).

For in vivo microCT, the specimen is immobilized and the x-ray source and detector rotate around the specimen. Multiple x-ray projections are collected and sections are computed from the projections. Sections can then be reconstructed into 3D representations. As in MRI, temporal gating is used to remove respiratory and sometimes circulatory artifacts.

Contrast in microCT is based on differences in x-ray absorption, so x-ray-dense hard tissues, such as bone, image particularly well. Air-filled spaces, such as lungs, also image well, owing to the much lower x-ray absorption relative to surrounding soft tissues. There is relatively little intrinsic x-ray density contrast between most soft tissues, so MRM is a better choice for soft tissue imaging. Extrinsic x-ray contrast agents may be injected and are particularly effective for vascular CT imaging. The time course of the appearance and disappearance of vascular contrast agents can be used in functional CT to estimate blood flow to an area (Lee 2002).

Synchrotron Beam Imaging

Synchrotron x-rays are generated by a particle accelerator in which charged particles travel around a ring at velocities near the speed of light to generate radiation in the form of an x-ray beam with high beam stability, high beam brilliance, and small particle beam emittance. Phase-enhanced x-ray imaging has been used to study a wide variety of samples, including sandpiles (Seeley et al. 2000), sea urchin teeth (Stock et al., 2003), automobile fuel injectors (Lee et al. 2001), and insect physiology (Westneat et al. 2003). Phase-enhanced x-ray imaging is based on the fact that the small x-ray source size and the relatively large distances from the source produce an x-ray beam that is partially coherent, allowing diffraction, edge enhancement, and impressive image quality (Cloetens et al. 1996). By using an x-ray scintillator, x-rays can be converted to visible light allowing images to be captured with a CCD video camera. This approach was recently used to examine movement in live insects (Westneat et al. 2003), allowing the discovery of a novel form of active tracheal ventilation in the respiratory system of insects. Still in the early stages of application to living organisms, synchrotron imaging holds promise for high-resolution (down to 1 μm), short-duration imaging of physiological processes and motions in small animals.

Ultrasound Microscopy

The resolution of ultrasound imaging can be increased by increasing the frequency of the sound pulses used, with maximum resolutions in the range of 50–100 μm (Turnbull and Foster 2002). The tradeoff is that higher frequency sounds are attenuated more quickly in tissues, so the higher frequency sounds used in high-resolution ultrasound microscopy imaging (typically 20–100 MHz) only penetrate 5–10 mm. As in clinical ultrasound imaging, backscattered sound echoes from the tissues are used to reconstruct a 2D section of an organism. Ultrasound is most commonly used for 2D imaging, but serial sections can be combined for 3D reconstructions (as in 3D echocardiography).

Ultrasound microscopy is most effective for imaging mouse and rat fetuses for in utero phenotype screens and for injections or other manipulations in utero. Spatial resolution is not as good as MRM, but temporal resolution is better. Ultrasound images in 2D can be collected at about 10 frames per second, which is high enough to allow real-time feedback for microinjection of mouse fetuses (Turnbull and Foster 2002). Ultrasound microscopy can also provide information on blood flow velocities through Doppler analysis of echoes from blood cells (Turnbull and Foster 2002).

Optical Coherence Tomography

Optical coherence tomography (OCT) is somewhat similar to ultrasound imaging, except that backscattered light rather than sound is used to produce 2D sections (Huang et al. 1991). Spatial resolution of OCT is up to 5 μm, an order of magnitude higher than ultrasound, and temporal resolution is similar to ultrasound. The use of long-wavelength light allows imaging to a depth of about 3 mm in semiopaque tissues, and considerably deeper in transparent tissues (Boppart et al. 2000).

OCT has been proposed as a good in vivo imaging method for amphibian embryos (Boppart et al. 2000), but it has not yet seen extensive use by developmental biologists.

As with ultrasound, the time resolution makes OCT a good method for guiding injections or measuring blood flow, but unlike ultrasound, it can not penetrate as deeply into tissue and may be less suitable for in utero studies of mammals. In clinical settings, OCT has become an important tool for imaging the eye and diagnosing retinal diseases such as macular degeneration. Miniature, endoscope-like OCT probes are beginning to be used in gastroenterology, cardiology, and oncology (Fujimoto et al. 1995).

Positron Emission Tomography

Positron emission tomography (PET) probably has limited application in developmental physiology owing to an inherent resolution limitation of about 1 mm. This resolution is sufficient for some imaging applications in small animals (Tai et al. 2001; Goertzen et al. 2002), but is not suitable for imaging early life stages of most species.

In PET imaging, a positron-emitting label, such as a chemical containing ^{16}O or ^{18}F, is injected into the subject. The label is preferentially taken up by some organs, indicating, for example, differences in blood flow or metabolism. Positrons are emitted from the label, each of which then travels in a random direction for some distance, up to 1 cm, before colliding with an electron and annihilating to produce two photons which then travel in opposite directions. A detector ring around the subject detects the photons, and the PET system calculates the 3D position of the annihilation event that produced each pair of photons. The resolution limitation comes from the random distance and direction that the positrons travel before annihilation; statistical methods can reduce this uncertainty to 1 mm, but it is difficult to see how the resolution of PET can be improved further. If the low resolution is not an issue, PET is an excellent method for physiological studies because blood flow, metabolism (by uptake of ^{18}F-labeled 2-fluorodeoxy-D-glucose), and other functions can be imaged in vivo, depending on the radionuclide-labeled chemical used. PET labels for gene expression are also being developed (Liang et al. 2002).

In Vivo Imaging in Developmental Physiology: Some Examples

Biomechanics of Segmented Musculature in Zebrafish Larvae

One of the defining characters of vertebrates and their close relatives is the presence of segmented axial musculature. In combination with a notochord or vertebral column to resist axial compression, contraction of the muscle segments on one side of the body produces axial bending. During steady swimming, waves of muscle activity pass down the body and interact with active and passive body stiffness to produce lateral undulatory movements.

The myomeres of adult fishes are so complex that laborious serial sectioning and 3D reconstruction are necessary to describe them adequately (Alexander 1969; Gemballa and Vogel 2002; van Leeuwen 1999; Wainwright 1983). However, during embryonic and larval development, myomeres begin as block-like myotomes with longitudinal muscle fibers, and then gradually develop the complex shape and muscle fiber trajectories of the adult (van Raamsdonk et al. 1974). We are using the relatively simple segmented musculature of larval zebrafish at 5 days post-fertilization (dpf) to study the relationship

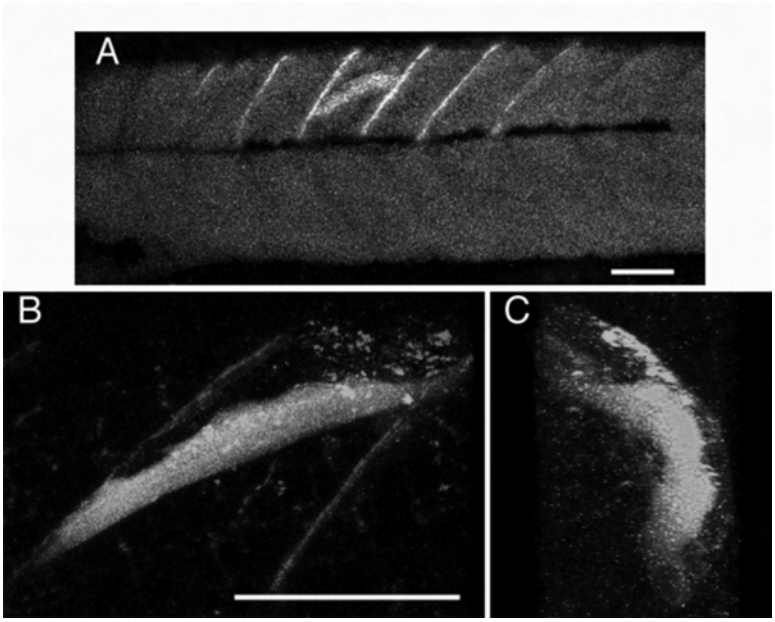

Figure 2.1 Muscle fibers in 5 days post-fertilization (dpf) zebrafish, imaged with confocal microscopy and microinjection of Texas Red dye. The head of the fish is to the left in panels A and B, and coming out of the page toward the viewer in panel C. (A) α-Actin GFP transgenic larva with one muscle fiber labeled by microinjection (10×). This is optical section 4 of 18 from a 230 μm deep stack taken from lateral to medial. Note that the myosepta also take up the Texas Red label. (B) Lateral projection of one muscle fiber in one myomere (63×). This lateral projection was reconstructed from a 71 μm deep stack of 75 optical sections. (C) 90° rotated view of panel B; transverse projection of one muscle fiber in one myomere. Scale bars = 100 μm.

between muscle fiber angle, myoseptal architecture, and biomechanical function (Brainerd and Azizi 2005).

In addition to the relative simplicity of their myomeres, larval zebrafish are also a good system for this work because their 3D muscle fiber angles and myomere shapes can be visualized by optical sectioning with laser scanning confocal microscopy. This technique is orders of magnitude faster than physical sectioning, yet produces high-resolution sections and 3D reconstructions of complex morphology. Furthermore, larvae can be immobilized in agar and imaged in vivo, thereby eliminating concerns about death and fixation artifacts.

We have quantified myomere morphology with in vivo confocal imaging (figures 2.1 and 2.2). Microinjection of Texas Red dye (10,000 MW, Molecular Probes) was used to label individual muscle fibers. Serendipitously, Texas Red injected into one myomere is also taken up by the adjacent myosepta, labeling them faintly (figure 2.1). Five days post-fertilization zebrafish were injected with Texas Red and allowed to incubate overnight under normal rearing conditions. Fish were imaged with a Zeiss LSM510 confocal microscope at 10× and 63×, and 3D reconstructions and measurements were made with the Zeiss Image Browser software.

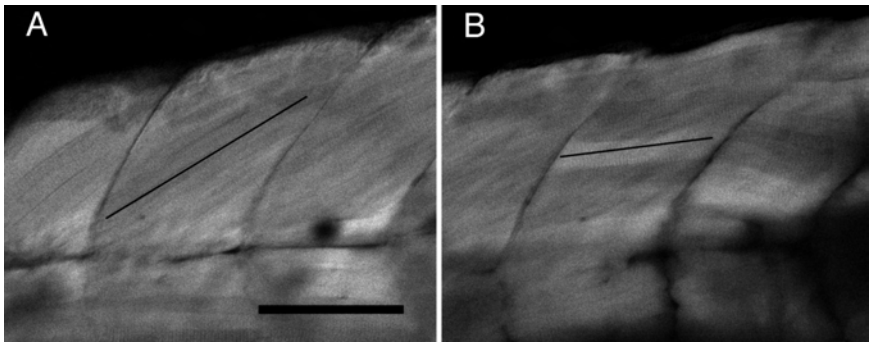

Figure 2.2 α-Actin GFP transgenic zebrafish, 5 dpf (63×). Thin black lines have been added to indicate muscle fiber angles. (A) Section 27 of 35 in a z-stack viewed from medial to lateral; muscle fiber angle = 27°. (B) Section 19 from the same z-stack; muscle fiber angle = 2°. Scale bar = 100 μm. Borders between muscle fibers and muscle striations are visible.

From the 3D reconstruction in figure 2.1B, some preliminary measurements have been made for this myomere and fiber: segment length, 98 μm; muscle fiber length, 176 μm; fiber diameter, 21.9 μm; muscle fiber angle formed with the horizontal plane, 25°; myoseptal angle formed with the horizontal plane, 43°. The muscle fiber angle formed with the sagittal plane can be measured by 90° rotation of the 3D reconstructed muscle fiber (figure 2.1C), but marked curvature of the fiber in this plane suggests that a simple angle measurement may not be adequate to describe the fiber trajectory.

Transgenic zebrafish in which green fluorescent protein (GFP) is coexpressed with α-actin were also used to image muscle fiber angles (figure 2.2). This technique has the advantage that multiple muscle fibers can be imaged and measured in one set of optical sections (z-series). In figure 2.2, two images from a z-series are shown, one superficial (lateral) section (A) and one deeper (more medial) section (B). For the superficial fibers, the muscle fiber angle formed with the horizontal plane is 27° (figure 2.2A), whereas the deeper fibers lie nearly in the horizontal plane, with angles of only 2° (figure 2.2B).

Alexander (1969) proposed that the function of heterogeneous muscle fiber angles within one segment is to produce similar muscle fiber strains in the medial and lateral portions of the myomere. If fiber angles were constant from medial to lateral, then medial muscle fibers located close to the neutral axis of bending (vertebral column in adult fishes; notochord in larvae) would shorten less than lateral fibers located closer to the skin. Alexander predicted that muscle fibers with low angles should lie near the neutral axis of the fish and fibers with high angles should be located more laterally.

This prediction is in agreement with our finding of lower fiber angles (2°) medially and higher angles (27°) laterally (figure 2.2). These differences in angle are in the correct direction to compensate for the differences in mediolateral position of these fibers, but are the differences in angle of the correct magnitude to compensate for their mediolateral positions as determined from position in the z-stack? The sections in figure 2.2 come from a 350 μm thick z-stack containing 35 sections (10 μm each) from the neutral axis to the lateral surface of a zebrafish larva. The section in figure 2.2B is number 19, so it is from an area 190 μm from the neutral axis, and the section in figure 2.2A is

section 27, so it is 270 μm from the neutral axis. Therefore the relative effect of these mediolateral positions is 270/190 = 1.42. This means that, for a given amount of lateral bending, the fibers in figure 2.2A would have to shorten (strain) by 1.42 times (42%) more than the fibers in figure 2.2B, if fiber angles were constant.

We can use a geometric model of segmented musculature to calculate whether the observed difference in fiber angle is sufficient to compensate for this predicted difference of 42% (Alexander 1969; Brainerd and Simons 2000; Azizi et al. 2002; Brainerd and Azizi 2005). If we assume that the segments bulge out equally in the dorsoventral and mediolateral directions (while shortening in the longitudinal direction; Alexander 1969; Azizi et al. 2002), then the effect of increasing muscle fiber angle from 2° medially to 27° laterally will be to increase the gear ratio from about 1 to 1.56. This means that, for a given longitudinal strain, the more angled fibers undergo 56% less strain, which more than compensates for the 42% greater strain that they experience as a result of being located farther from the neutral axis.

This preliminary result is based on a 2D, planar model of segmented musculature (Azizi et al. 2002). As shown in figure 2.1C, however, muscle fibers are angled and curved in the sagittal as well as the frontal plane. A 3D model that includes muscle fiber curvature, and not just angles, will be required for a more complete understanding of segmented muscle function in larval zebrafish (Brainerd and Azizi 2005).

Neural Control of Movement in Zebrafish Larvae

The control of movement has been a major focus of systems neuroscience. Electrophysiology in animals, including lamprey (e.g., Grillner et al. 1995, 1998; Buchanan 1996), goldfish (e.g., Fetcho and Faber 1988; Eaton et al. 2001), tadpole (e.g., Roberts et al. 1998; Yoshida et al. 1998), turtles (e.g., Stein et al. 1995; Currie and Gonsalves 1999), and rodents (e.g., Kjaerulff and Kiehn 1997; Kremer and Lev Tov 1997), have provided models for the organization of spinal cord circuits involved in locomotor generation and startle behaviors. In recent years another vertebrate system, the zebrafish, has been added to this list (Fetcho and O'Malley 1995; O'Malley et al. 1996; Fetcho et al. 1998). As discussed by Fetcho and Liu (1998) and illustrated below, the zebrafish system has a number of characteristics that are favorable for such work and complement more traditional approaches. Foremost among these advantages is that the body of the larval zebrafish is transparent, making it possible to image neuron morphology and function in the intact, live animal. In addition, because the zebrafish is a widely studied developmental and genetic model, an array of powerful genetic approaches are available for zebrafish that can aid our exploration of the nervous system and its physiology.

Recently, confocal imaging has provided new, less invasive approaches to examine motor control. Because confocal approaches can be used in vivo, they are particularly amenable to studies of physiology. Because they are used on small animals (e.g., zebrafish examined are around 5 mm in total length), early developmental periods that may be difficult to access with traditional neurophysiology may be the most amenable subjects for imaging approaches. Neural imaging can be used while maintaining the health of the animal during repeated measures, as may be necessary to track morphology and function through development. Lastly, because the morphology of neurons can be assessed prior to recording their physiology and many cells can be imaged simultaneously, imaging can be targeted to a specific cell type or population.

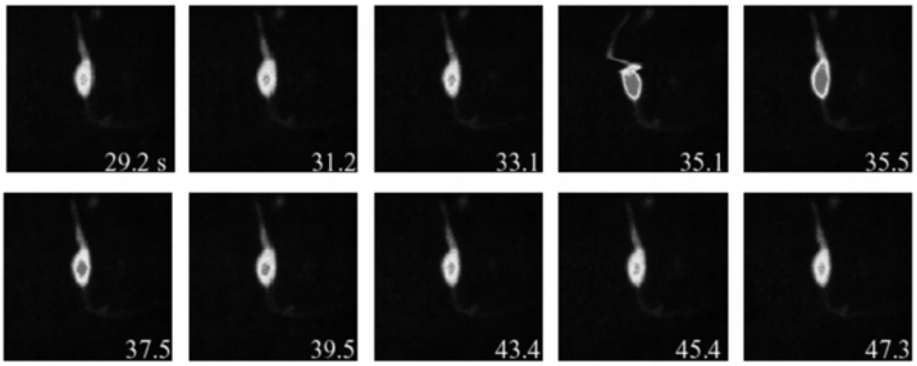

Figure 2.3 A Mauthner neuron from dorsal view in a larval zebrafish (5 dpf) labeled with Calcium Green Dextran (10,000 MW) imaged with confocal microscopy (10× lens). The cell is shown in pseudocolor applied by Zeiss 510 confocal software to color code the brightness of the cell, from deep blue at low fluorescent brightness to red at the peak brightness recorded (as reproduced here in grayscale, the red appears as a dark spot in the center of the cell with a bright halo around it). The brightest focal plane of the cell is imaged so as not to overestimate the response due to a change in the position of the cell. Successive images show a portion of a time series that illustrates the change in brightness of the cell during a response. The cell is at rest until 35.1 s, at which time a tactile startle stimulus, a touch to the head, is applied. The shift in cell position is combined passive movement due to the stimulus and active movement of the animal during the response. In the same frame, a dark spot appears at the center of the Mauthner cell indicating that the cell was active. The slow decrease in fluorescence after the response does not indicate continued activity of the cell but rather calcium dissociation from the dye and sequestering. Imaging in this figure was particularly slow because of the large size of each frame and resolution taken.

Confocal neural imaging as an in vivo physiology technique in zebrafish was initially developed by Fetcho, O'Malley, and colleagues to image the activity of motoneurons and hindbrain neurons during locomotion (Fetcho and O'Malley 1995; O'Malley et al. 1996; Fetcho et al. 1998). Physiological imaging had been previously developed (O'Donovan et al. 1993; McClellan et al. 1994; Lev-Tov and O'Donovan 1995) for studies of isolated spinal cord, and the zebrafish work extended the preparation to whole-animal studies. The primary indicators of cell activity used in imaging are fluctuations in cell calcium levels during activity.

In the most common method of calcium imaging, neurons are retrogradely labeled with calcium indicator dyes such as Calcium Green Dextran (Molecular Probes). Dye is injected into the axon and taken up along the axon to the cell body. Calcium Green Dextran becomes brighter in interaction with calcium; therefore, when there is an increase in cytosolic intracellular calcium during cell activity, the cell appears brighter. Brightness is then recorded with confocal microscopy and pseudo-color coded, generally with higher fluorescence brightness values indicated by more orange and red pixels. Figure 2.3 shows an example of calcium imaging of activity in a Mauthner neuron, a reticulospinal cell that functions in startle behavior, responding to a touch startle stimulus. The application of the stimulus is indicated by the movement artifact at 35.1 s. In that same frame the response of the cell is evident from the change in brightness of the cell body, indicated by the color shift from yellow to red.

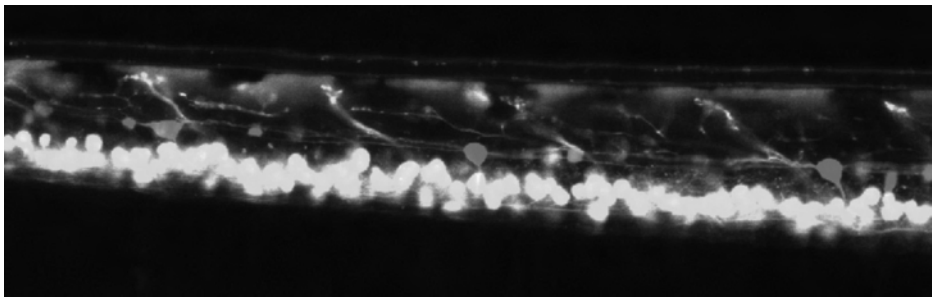

Figure 2.4 A section of trunk spinal cord imaged with confocal microscopy in lateral view in a 5–7 dpf zebrafish larva (10×). White cells are motoneurons expressing green fluorescent protein under the control of the islet-1 promoter. Gray cells are commissural primary ascending (CoPA) interneurons that were labeled with Texas Red Dextran (10,000 MW) by microinjection into the spinal cord. Microinjection and transgenic approaches can be used independently or in combination to examine the morphology of neurons.

While calcium imaging is temporally limited by the reuptake of the calcium and by the imaging rate of the confocal as described previously, it can give clear evidence of the stimuli to which a cell does or does not respond.

In some of the first zebrafish calcium imaging experiments, O'Malley and colleagues (1996) used this approach to identify the roles of descending reticulospinal neurons, including the Mauthner cell (figure 2.3) and its serial homologs MiD2 and MiD3, in startle response behavior. They imaged the responses of the cells to touch stimulation applied to the head or to the tail of the animal. They found that while all three cells responded to a head touch, only the Mauthner cells responded to a tail touch. These experiments illustrate the value of calcium imaging to examine subtle differences in cell activity among multiple cells in a single preparation.

Neural imaging has been extended to examine cells that had not previously been clearly identified as motoneurons and reticulospinal cells. Hale et al. (2001) surveyed interneuron cell types in the larval zebrafish spinal cord, describing several new cell types and providing information on their distribution in the cord, adding to previous morphological study in fixed tissue (Bernhardt et al. 1990). Because the in vivo imaging approach allows for rapid 3D reconstruction of morphology, the nervous system can be surveyed rapidly and basic characteristics of cell morphology assessed, such as axon lengths and trajectories, number of cells of a given cell type, cell body size, and position in the spinal cord. Transgenic fish in which green fluorescent protein is expressed in neurons either transiently or in stable lines (e.g., Higashijima et al. 2000) will greatly augment such work because finer features of morphology and local cells may be visualized (figure 2.4).

To correlate the activity of spinal interneurons with behavior, Ritter et al. (2001) developed a semiembedded preparation to record simultaneously the activity of neurons with confocal microscopy and body movements with high-speed video. They embedded the rostral portion of the animal in agar to stabilize it for confocal imaging while leaving the tail free in water. By placing a high-speed video camera over the confocal stage, they were able to record the movements of the tail in response to a variety of

stimuli and to correlate movement with the activity of the neurons. With this preparation, Ritter and colleagues (2001) examined the responses of two interneuron cell types, CiD (circumferential descending) and MCoD (multipolar commissural descending) interneurons, in startle and swim behaviors. They found that CiD cells, which are believed to be homologous to the excitatory startle interneurons of goldfish (Fetcho and Faber 1988), function in the startle response but are not active in steady swimming, whereas MCoDs show the converse pattern.

Recently, imaging neuron physiology has been extended to populations of interneurons. Bhatt and colleagues (pers. comm.) have shown that it is possible to assess activity in many cells of a given class of neurons simultaneously, determining differences in cell activity to alternative stimuli. Ratiometric imaging has been essential for this approach. By labeling cells with both a calcium-sensitive dye and a control dye that does not respond to calcium, changes in the position of cells due to movement artifact can be factored into calculations of brightness levels. This is particularly important when the optimal focal plane (the brightest focal plane at rest) varies among the cells to be imaged together. Other new approaches to physiological imaging are providing exciting opportunities for more specific imaging. For example, GFP-tagged calcium/calmodulin-dependent protein kinase II translocation can be visualized at excitatory synapses in response to stimulation (Gleason et al. 2003).

Understanding cell morphology and cell activity during behavior makes it possible to hypothesize roles for those cells in movement. To test those roles, one critical approach has been cell ablation. Because we can visualize cells in vivo, it is possible to focus a laser precisely on the cell and kill it either by disrupting internal structure or with the dye's phototoxicity. Alternatively, axon severing can be used to disrupt normal cell connections in large numbers of cells simultaneously (Gahtan and O'Malley 2001). Unlike traditional approaches, such as chemical lesion, which disrupt a region of the central nervous system, single cell targeting prevents damage to the tissue around the targeted cells. Figure 2.5 demonstrates MCoD cells in a region of the cord prior to ablation (top) and after those cells were individually lesioned. Note that the Mauthner axon and other cells labeled in the image are intact and do not appear to have changed in morphology.

By testing the behavior of the animal before and after the ablation, we can assess how the ablated cells influence behavior. Because of the concern over other damage, multiple controls are critical for this type of experiment. An excellent example of ablations used to test function is work by Liu and Fetcho (1999), in which they ablated the Mauthner cell to test its role in startle behavior. They found that, contrary to expectations, the lesion of the Mauthner cell did not change the performance of the startle elicited by stimulus directed at the head of the animal. However, it did result in a decrease in response to tail stimuli. When the Mauthner cell and its serial homologs, MiD2 and MiD3, were ablated, response to head stimuli decreased, demonstrating that reticulospinal cells other than the Mauthner neurons are critical to a high-performance startle response.

Concluding Remarks

In vivo and functional imaging techniques provide opportunities for developmental physiologists to integrate levels of study from gene expression to the physiological performance and behavior of whole organisms. Integrated studies of morphological and

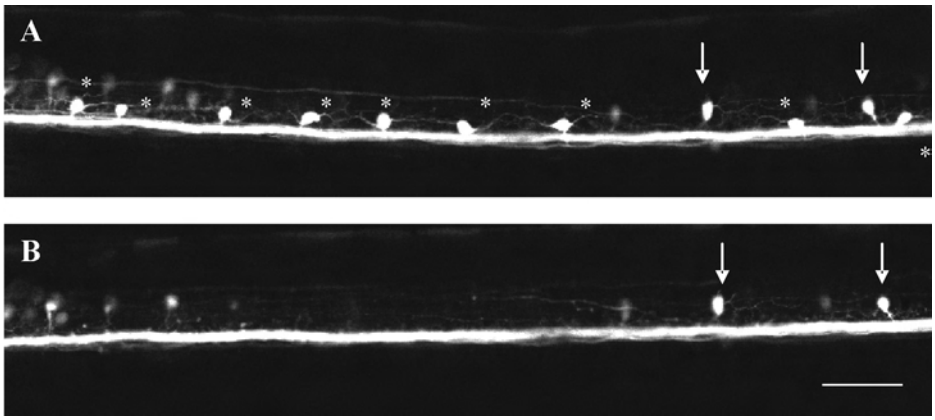

Figure 2.5 A section of trunk spinal cord in lateral view from a 5–7 dpf zebrafish larva imaged with confocal microscopy (10×). Cells are labeled with fluorescein dextran (10,000 MW, Molecular Probes) by microinjection into the spinal cord. (A) Preablation image. The nine squat cells marked with asterisks are multipolar commissural descending (MCoD) interneurons. MCoD cell bodies lie immediately dorsal to the Mauthner cell axon, the white stripe in the images. Several cells of another cell type are marked with arrows. (B) Postablation image. The same region of spinal cord after the MCoD cells were killed with a short burst of light from a nitrogen pulse laser. Although all the MCoDs are gone, other cells shown in the preablation image (A) and the Mauthner cell axon remain intact and do not appear damaged. Scale bar = 50 μm.

physiological development are particularly facilitated by imaging, raising the possibility of bringing more physiology into the field of evolutionary developmental biology, which to date has focused mostly on morphology.

The most broadly useful imaging techniques for developmental physiology currently are widefield photomicroscopy, videomicroscopy, and confocal microscopy. Ultrasound and MR microscopy are useful for studies of inaccessible bird and mammalian embryos, and microCT is good for imaging skeletal and lung structures. Most techniques are limited in their ability to collect images with high spatial resolution quickly, so time resolution of image series, particularly if z-stacks of images are needed for 3D reconstruction, is often lower than would be ideal for physiological studies.

Multidimensional images contain enormous amounts of information, and may be useful to several different investigators for different purposes. The developmental physiology community would be well served by agreeing quickly on standards for image data and metadata, to facilitate archiving and the creation of a public database for developmental physiology images. The success of GenBank and other public databases demonstrates the power of such communal resources to promote efficient and effective use of research results.

Acknowledgments This material is based upon work supported by the U.S. National Science Foundation under grants 0316174 (to ELB) and 0238464 (to MEH) and by a U.S. National Institutes of Health grant NS043977 to MEH. Thanks to M. Westneat for help with the synchrotron imaging section, and to D. Callaham and P. Wadsworth for help with the microscopy sections.

References

Alexander RM (1969). The orientation of muscle fibers in the myomeres of fishes. *Journal of the Marine Biology Association U.K.*, 49, 263–290.

Alley MT, Napel S, Amano Y, et al. (1999). Fast 3d cardiac cine MR imaging. *Journal of Magnetic Resonance Imaging*, 9, 751–755.

Azizi E, Gillis GB, and Brainerd EL (2002). Morphology and mechanics of myosepta in a swimming salamander. *Comparative Biochemistry and Physiology*, *Part A*, 133, 967–978.

Barinaga M (2003). Still debated, brain image archives are catching on. *Science*, 300, 43–45.

Barresi MJ, D'Angelo JA, Hernandez LP, and Devoto SH (2001). Distinct mechanisms regulate slow-muscle development. *Current Biology*, 11, 1432–1438.

Bernhardt RR, Chitnis AB, Lindamer L, and Kuwada JY (1990). Identification of spinal interneurons in the embryonic and larval zebrafish. *Journal of Comparative Neurology*, 302, 603–616.

Boppart SA, Brezinski ME, and Fujimoto JG (2000). Optical coherence tomography imaging in developmental biology. *Methods in Molecular Biology*, 135, 217–233.

Brainerd EL and Azizi E (2005). Muscle fiber angle, segment bulging and architectural gear ratio in segmented musculature. Journal of Experimental Biology, 208, 3249–3261.

Brainerd EL and Simons RS (2000). Morphology and function of the lateral hypaxial musculature in salamanders. *American Zoologist*, 40, 77–86.

Buchanan JT (1996). Lamprey spinal interneurons and their role in swimming activity. *Brain Behavior and Evolution*, 48, 287–296.

Bulte JWM, van Zijl PCM, and Mori S (2002). Magnetic resonance microscopy and histology of the CNS. *Trends in Biotechnology*, 20, S24–S28.

Chen XJ, Chawla MS, Hedlund LW, Moeller HE, MacFall JR, and Johnson GA (1998). MR microscopy of lung airways with hyperpolarized ^{3}He. *Magnetic Resonance Medicine*, 39, 79–84.

Chudakov DM, Belousov VV, Zaraisky AG, et al. (2003). Kindling fluorescent proteins for precise in vivo photolabeling. *Nature*, 21, 191–194.

Cloetens P, Barrett R, Baruchel J, Guigay J, and Schlenker M (1996). Phase objects in synchrotron radiation hard x-ray imaging. *Journal of Physics D* (*Applied Physics*), 29, 133–146.

Currie SN and Gonsalves GG (1999). Reciprocal interactions in the turtle hindlimb enlargement contribute to scratch rhythmogenesis. *Journal of Neurophysiology*, 81, 2977–2987.

DeClerck N, van Dyck D, and Postnov AA (2003). Non-invasive high-resolution μCT of the inner structure of living animals. *Microscopy and Analysis* (*The Americas*), 58, 9–11.

Dubertret B, Skourides P, Norris DJ, Noireaux V, Brivanlou AH, and Libchaber A (2002). In vivo imaging of quantum dots encapsulated in phospholipid micelles. *Science*, 298, 1759–1762.

Eaton RC, Lee RKK, and Foreman MB (2001). The Mauthner cell and other identified neurons of the brainstem escape network of fish. *Progress in Neurobiology*, 63, 467–485.

Fenster A (2002). A Trends guide to imaging technologies. *Trends in Biotechnology*, 20, S1–S2.

Fetcho JR and Faber DS (1988). Identification of motoneurons and interneurons in the spinal network for escapes initiated by the Mauthner cell in goldfish. *Journal of Neuroscience*, 8, 4192–4213.

Fetcho JR and Liu KS (1998). Zebrafish as a model system for studying neuronal circuits and behavior. *Annals of the New York Academy of Sciences*, 860, 333–345.

Fetcho JR and O'Malley DM (1995). Visualization of active neural circuitry in the spinal cord of intact zebrafish. *Journal of Neurophysiology*, 73, 399–406.

Fetcho JR, Cox KJA, and O'Malley DM (1998). Monitoring activity in neuronal populations with single-cell resolution in a behaving vertebrate. *Histochemical Journal*, 30, 153–167.

Fujimoto JG, Brezinski ME, Tearney GJ, et al. (1995). Biomedical imaging and optical biopsy using optical coherence tomography. *Nature Medicine*, 1, 970–972.

Gahtan E and O'Malley DM (2001). Rapid lesioning of large numbers of identified vertebrate neurons: applications in zebrafish. *Journal of Neuroscience Methods*, 108, 97–110.

Gemballa S and Vogel F (2002). Spatial arrangements of white muscle fibers and myoseptal tendons in fishes. *Comparative Physiology and Biochemistry*, *Part A*, 133, 1013–1037.

Gleason MR, Higashijima S, Dallman J, Liu K, Mandel G, and Fetcho JR (2003). Translocation of CaM kinase II to synaptic sites in vivo. *Nature Neuroscience*, 63, 217–218.

Goertzen AL, Meadors AK, Silverman RW, and Cherry SR (2002). Simultaneous molecular and anatomical imaging of the mouse in vivo. *Physics in Medicine and Biology*, 47, 4315–4328.

Goldman ER, Anderson GP, Tran PT, Mattoussi H, Charles PT, and Mauro JM (2002). Conjugation of luminescent quantum dots with antibodies using an engineered adaptor protein to provide new reagents for fluoroimmunoassays. *Analytical Chemistry*, 74, 841–847.

Grillner S, Deliagina T, Ekeberg O, et al. (1995). Neural networks that co-ordinate locomotion and body orientation in lamprey. *Trends in Neuroscience*, 18, 270–279.

Grillner S, Parker D, and El Manira A (1998). Vertebrate locomotion—a lamprey perspective. *Annals of the New York Academy of Sciences*, 860, 1–18.

Hale ME, Ritter DA, and Fetcho JR (2001). A confocal study of spinal interneurons in living larval zebrafish. *Journal of Comparative Neurology*, 437, 1–16.

Hanken J, Klymkowsky MW, Summers CH, Seufert DW, and Ingebrigtsen N (1992). Cranial ontogeny in the direct-developing frog, *Eleutherodactylus coqui* (Anura: Leptodactylidae), analyzed using whole-mount immunohistochemistry. *Journal of Morphology*, 211, 95–118.

Hernandez LP, Barresi MJF, and Devoto SH (2002). Functional morphology and developmental biology of zebrafish: reciprocal illumination from an unlikely couple. *Integrative and Comparative Biology*, 42, 222–231.

Higashijima S, Okamoto H, Ueno N, Hotta Y, and Eguchi G (1997). High-frequency generation of transgenic zebrafish which reliably express GFP in whole muscles or the whole body using promotors of zebrafish origin. *Developmental Biology*, 192, 189–199.

Higashijima S, Hotta Y, and Okamoto, H (2000). Visualization of cranial motor neurons in live transgenic zebrafish expressing green fluorescent protein under the control of the *Islet-1* promoter/enhancer. *Journal of Neuroscience*, 20, 206–218.

Holdsworth DW and Thornton MM (2002). Micro-CT in small animal and specimen imaging. *Trends in Biotechnology*, 20, S34–S39.

Hove JR, Köster RW, Forouhar AS, Acevedo-Bolton G, Fraser SE, and Gharib M (2003). Intracardiac fluid forces are an essential epigenetic factor for embryonic cardiogenesis. *Nature*, 421, 172–177.

Huang D, Swanson EA, Lin CP, et al. (1991). Optical coherence tomography. *Science*, 254, 1178–1181.

Jacobs RE and Fraser SE (1994). Magnetic resonance microscopy of embryonic cell lineages and movements. *Science*, 263, 681–684.

Kjaerulff O and Kiehn O (1997). Crossed rhythmic synaptic input to motoneurons during selective activation of the contralateral spinal locomotor network. *Journal of Neuroscience*, 17, 9433–9447.

Kremer E and Lev Tov A (1997). Localization of the spinal network associated with generation of hindlimb locomotion in the neonatal rat and organization of its transverse coupling system. *Journal of Neurophysiology*, 77, 1155–1170.

Lee T (2002). Functional CT: physiological models. *Trends in Biotechnology*, 20, S3–S10.

Lee WK, Fezzaa K, and Wang J (2001). X-ray propagation-based phase-enhanced imaging of fuel injectors. *ASME Internal Combustion Engine Division*, *Fall Technical Conference*.

Lev-Tov A and O'Donovan MJ (1995). Calcium imaging of motoneuron activity in the en-bloc spinal cord preparation of the neonatal rat. *Journal of Neurophysiology*, 74, 1324–1334.

Liang Q, Gotts J, Satyamurthy N, et al. (2002). Non-invasive, repetitive, quantitative measurement of gene expression from a bicistronic message by positron emission tomography, following gene transfer with adenovirus. *Molecular Therapy*, 6, 73–82.

Liu KS and Fetcho JR (1999). Laser ablations reveal functional relationships of segmental hindbrain neurons in zebrafish. *Neuron*, 23, 325–335.

Logothetis NK, Pauls J, Augath M, Trinath T, and Oeltermann A (2001). Neurophysiological investigation of the basis of the fMRI signal. *Nature*, 412, 150–157.

Louie AY, Huber MM, Ahrens ET, et al. (2000). In vivo visualization of gene expression using magnetic resonance imaging. *Nature Biotechnology*, 18, 321–325.

MacLaren DC, Toyokuni T, Cherry SR, et al. (2000). PET imaging of transgene expression. *Biological Psychiatry*, 48, 337–348.

Marx V (2002). Beautiful bioimages for the eyes of many beholders. *Science*, 297, 39–40.

McClellan AD, McPherson D, and O'Donovan MJ (1994). Combined retrograde labeling and calcium imaging in spinal cord and brainstem neurons of the lamprey. *Brain Research*, 663, 61–68.

O'Connell-Rodwell CE, Burns SM, Bachmann MH, and Contag CH (2002). Bioluminescent indicators for in vivo measurements of gene expression. *Trends in Biotechnology*, 20, S19–S23.

O'Donovan MJ, Ho S, Sholomenko G, and Yee W (1993). Real time imaging of neurons retrogradely and anterogradely labelled with calcium sensitive dyes. *Journal of Neuroscience Methods*, 46, 91–106.

O'Malley DM, Kao Y-H, and Fetcho JR (1996). Imaging the functional organization of zebrafish hindbrain segments during escape behaviors. *Neuron*, 17, 1145–1155.

Ritter DA, Bhatt DH, and Fetcho JR (2001). In vivo imaging of zebrafish reveals differences in the spinal networks for escape and swimming movements. *Journal of Neuroscience*, 21, 8956–8965.

Roberts A, Soffe SR, Wolf ES, Yoshida M, and Zhao F-Y (1998). Central circuits controlling locomotion in young frog tadpoles. *Annals of the New York Academy of Sciences*, 860, 19–34.

Schwerte T, Überbacher D, and Pelster B (2003). Non-invasive imaging of blood cell concentration and blood distribution in zebrafish *Danio rerio* incubated in hypoxic conditions in vivo. *Journal of Experimental Biology*, 206, 1299–1307.

Seeley LH, Kim KH, Behne EA, et al. (2000). Granule-by-granule reconstruction of a sandpile from x-ray microtomography data. *Physical Review*, 62, 8175–8181.

Seydel C (2003). Quantum dots get wet. *Science*, 300, 80–81.

Sharpe J, Ahlgren U, Perry P, et al. (2002). Optical projection tomography as a tool for 3D microscopy and gene expression studies. *Science*, 296, 541–545.

Shotton DM (2000). From image to knowledge: the state of the art in image bioinformatics. *Microscopy and Analysis*, November 2000, 23–25.

Stein PSG, Victor JC, Field EC, and Currie SN (1995). Bilateral control of hindlimb scratching in the spinal turtle: contralateral spinal circuitry contributes to the normal ipsilateral motor pattern of fictive rostral scratching. *Journal of Neuroscience*, 15, 4343–4355.

Stephens DJ and Allan VJ (2003). Light microscopy techniques for live cell imaging. *Science*, 300, 82–86.

Stock SR, Dahl T, Barss J, Veiss A, Fezzaa K, and Lee WK (2003). Mineral phase microstructure in teeth of the short spined sea urchin (*Lytechinus variegatus*): studies with x-ray phase contrast imaging and with absorption microtomography. *Advances in X-ray Analysis*, 47.

Stuart GW, McMurray JV, and Westerfield M (1998). Replication, integration and stable germ line transmission of foreign sequences injected into early zebrafish embryos. *Development*, 103, 403–412.

Swedlow JR, Goldberg I, Brauner E, and Sorger PK (2003). Informatics and quantitative analysis in biological imaging. *Science*, 300, 100–102.

Tai YC, Chatziioannou AF, Siegal S, et al. (2001). Performance evaluation of the microPET P4: a PET system dedicated to animal imaging. *Physics in Medicine and Biology*, 46, 1845.

Turnbull DH and Foster FS (2002). In vivo ultrasound biomicroscopy in developmental biology. *Trends in Biotechnology*, 20, S29–S33.

van Leeuwen JL (1999). A mechanical analysis of myomere shape in fish. *Journal of Experimental Biology*, 202, 3405–3414.

van Raamsdonk W, van der Stelt A, Diegenbach PC, et al. (1974). Differentiation of the musculature of the teleost *Brachydanio rerio*. I. Myotome shape and movements in the embyro. *Zeitschrift Anatomischer Entwicklungs-Geschichte*, 145, 321–342.

Wainwright SA (1983). To bend a fish. In PW Webb and D Weihs (eds.), *Fish Biomechanics*, Praeger, New York.

Westneat MW, Betz O, Blob RW, Fezzaa K, Cooper WJ, and Lee W-K (2003) Tracheal respiration in insects visualized with synchrotron x-ray imaging. *Science*, 299, 558–560.

Yoshida M, Roberts A, and Soffe SR (1998). Axon projections of reciprocal inhibitory interneurons in the spinal cord of young *Xenopus* tadpoles and implications for the pattern of inhibition during swimming and struggling. *Journal of Comparative Neurology*, 400, 504–518.